Pairing symmetry of interacting fermions on a twisted bilayer graphene superlattice

Huaiming Guo, Xingchuan Zhu, Shiping Feng, and Richard T. Scalettar

Phys. Rev. B **97**, 235453 — Published 29 June 2018

DOI: 10.1103/PhysRevB.97.235453

The Hubbard Model on a Triangular Lattice: Unconventional superconductivity with a nearly flat band

Huaiming Guo[1], Xingchuan Zhu[2], Shiping Feng[2], and Richard T. Scalettar[3]
[1]*Department of Physics, Key Laboratory of Micro-Nano Measurement-Manipulation and Physics (Ministry of Education), Beihang University, Beijing, 100191, China*
[2]*Department of Physics, Beijing Normal University, Beijing, 100875, China and*
[3]*Physics Department, University of California, Davis, Ca 95616, USA*

The pairing symmetry of the Hubbard Hamiltonian on a triangle lattice with a nearly-flat low energy band is studied with the determinant quantum Monte Carlo method. We show that the low temperature phase is insulating at half-filling, even for relatively weak interactions. The natures of the spin and pairing correlations upon doping are determined, and exhibit an electron-hole asymmetry. Among the pairing symmetries allowed, we demonstrate that the dominating channels are d-wave, opening the possibility of condensation into an unconventional $d_{x^2-y^2}+id_{xy}$ phase, which is characterized by an integer topological invariant and gapless edge states. The results are closely related to the correlated insulating phase and unconventional superconductivity discovered recently in twisted bilayer graphene.

Introduction- Over the last decade, studies of bilayer and rotated layer graphene have revealed a wealth of information concerning the modifications to the Dirac band structure of a single honeycomb lattice which result from interlayer hybridization $t_\perp$. Much of the initial work[1–3] explicitly tackled the very large unit cells associated with small twist angles θ. Although Bernal (AB) stacked bilayers lose linear dispersion and chirality properties, it was shown that these can be restored at other twist angles. For intermediate $2^\circ < \theta < 15^\circ$, for example, Dirac bands with a renormalized velocity persist. These calculations helped clarify experimental observations of graphene-like properties even in materials with large numbers of planes[4–9], far from the single-layer graphene limit.

Beyond the continued presence of Dirac dispersion, two other fundamental conclusions were drawn for twisted graphene bilayers. First, at certain 'magic angles,' flat bands are formed from the merger of van Hove singularities on either side of the Dirac point[2]. Second, associated with these flat bands, electronic states become confined in the 'AA' regions of the Moiré pattern formed by the rotation,

Along with these band structure investigations, the effects of interlayer hybridization on magnetic and superconducting properties in the presence of an on-site Hubbard interaction U were explored[10–14]. In a single honeycomb layer there is a critical value $U_c/t \sim 3.87$[15,16] for the onset of antiferromagnetic long range order (AFLRO). For Bernal (AB) bilayer stacking, at $t_\perp = t$, it was shown that $U_c/t \sim 2.2$[11], and is accompanied by the opening of a single particle gap $\Delta_{\rm sp}$ at a roughly comparable U/t. The presence of sites with different coordination numbers, $z = 3$ and $z = 4$, lends an additional richness to the magnetic behavior, as does the possibility of quenching AFLRO through interlayer singlet formation in the (unphysical) regime of larger $t_\perp$.

These explorations of band structure and magnetism lay an essential foundation for the very recent discovery of unconventional superconductivity in magic angle graphene bilayers[17,18], which themselves already build on work on novel pairing in single layers[19,20]. Indeed, the understanding of the Moiré triangular superlattice of AA and AB sites provides a possible approach to the understanding of pairing in these systems based on effective Hamiltonians which treat extended AA and AB regions as 'sites' of a simplified model.

This approach underlies a recent paper which considers topological superconductivity in a two orbital Hubbard model on a triangular lattice[21]. Importantly, it opens the door to the use of Quantum Monte Carlo (QMC) methods, which can provide an exact treatment of correlated electron physics, but are limited to lattices of finite size, and are unfeasible for direct treatment of the immense unit cells at small θ. Despite the sign problem[22–24], QMC approaches provided an early, essential clue concerning d-wave pairing in the single band Hubbard Hamiltonian on a square lattice[25–27], and hence, if applicable to an appropriate description of bilayer graphene, might similarly lend important insight.

In this paper, we apply QMC approaches to the Hubbard Hamiltonian on a triangle lattice with a nearly-flat low energy band, which yield results sharing interesting features with those observed experimentally[17,18]. Our key conclusions are: (i) a correlated insulator arises at half-filling even at relatively small values of U/t; (ii) the dominant pairing symmetry is d-wave, degenerate in the x^2-y^2 and xy channels, opening the possibility of a chiral phase; (iii) (short range) antiferromagnetic fluctuations are present and on sites participating in the flat band are significantly stronger below half-filling ($\rho = 1$) than above. Finally, (iv) the tendency to superconductivity is also asymmetric, with a stronger response to doping below half-filling.

In the remainder of this paper we describe our effective model, providing some additional motivation, discuss its band structure, and present the qualitative physics within mean field theory, along with the associated topo-

logical properties. We then turn the results of DQMC for the Mott gap and magnetic correlations, and, finally, superconductivity.

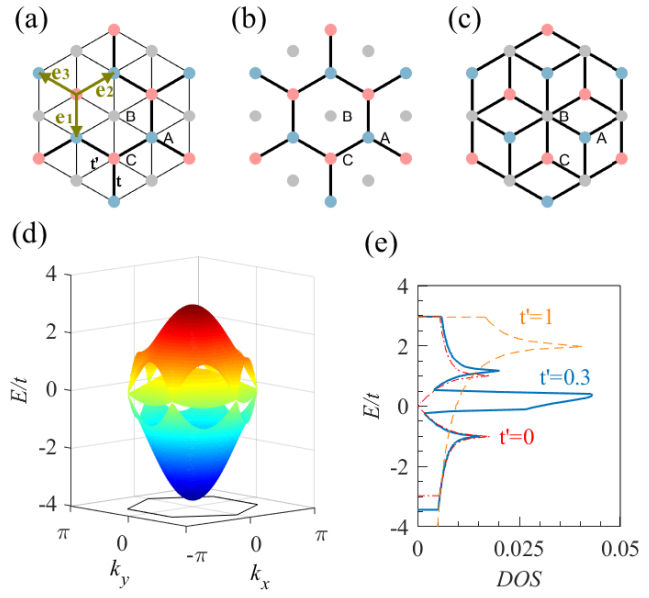

FIG. 1. (a): The effective lattice which results from treating each AA region as an effective 'site' connected by modulated hopping amplitudes. Three elementary vectors $\mathbf{e}_{1,2,3}$, the A, B, C sublattices are indicated. (b): The honeycomb lattice in the limit $t' = 0$. (c): The dice lattice in the limit $t = 0$. (d): The band structure of the effective model in the first Brillouin zone. (e): The density of states corresponding to the band shown in (d). In (e) we also show the density of states of the limiting cases of the triangular ($t' = t$) lattice and hexagonal ($t' = 0$) lattice. In the latter case, we do not show the δ-function peak at $E/t = 0$. In (d) and (e), the anisotropic factor $t'/t = 0.3$.

The effective Model- Twisted bilayer graphene has been found to have nearly flat low-energy bands for special discrete angles, where the Moiré pattern is a superlattice comprised of AA and $AB(BA)$ stacking regions[28–32]. The wave function is highly concentrated in the AA regions and is associated with a band with weak dispersion. A correlated insulator is found at half filling[17]. These considerations suggest the possibility of simulating each AA region as a 'site' in an effective model which includes a charging energy penalty for occupation of AA regions, and result in an effective Hubbard Hamiltonian on a triangle geometry with modulated hoppings giving rise to a nearly flat low energy band,

$$H = -\sum_{\langle lj\rangle\sigma} t_{lj} c^\dagger_{j\sigma} c_{l\sigma} + U \sum_i \left(n_{i\uparrow} - \frac{1}{2}\right)\left(n_{i\downarrow} - \frac{1}{2}\right). \quad (1)$$

Here $c^\dagger_{j\sigma}$ and $c_{j\sigma}$ are the creation and annihilation operators, respectively, at site j with spin $\sigma =\uparrow,\downarrow$. $n_{i\sigma} = c^\dagger_{i\sigma} c_{i\sigma}$ is the number of electrons of spin σ on site i, and U is the on-site repulsion. The modulation t, t' can be understood by a constuction which begins with a honeycomb lattice with hopping t and then adding a site at the center of each hexagon in the honeycomb lattice. These sites are linked with hopping t' to their six near neighbors. See Fig. 1(a), (b). Throughout the paper we set to $t = 1$ as the unit of energy.

The modified triangle lattice has a three-site unit cell. In momentum space, the $U = 0$ Hamiltonian is,

$$\mathcal{H}_0(\mathbf{k}) = \begin{pmatrix} 0 & -t\gamma_{\mathbf{k}} & -t'\gamma^*_{\mathbf{k}} \\ -t\gamma^*_{\mathbf{k}} & 0 & -t'\gamma_{\mathbf{k}} \\ -t'\gamma_{\mathbf{k}} & -t'\gamma^*_{\mathbf{k}} & 0 \end{pmatrix}, \quad (2)$$

with $\gamma_{\mathbf{k}} = \sum_j e^{i\mathbf{k}\cdot\mathbf{e}_j}$ $(j = 1, 2, 3)$. The spectrum can be directly obtained and contains three branches, as shown in Fig. 1(c), (d). The upper and lower bands have significant dispersion, while the middle band has a narrow width, with a flatness that can be continuously tuned by t'. At either extreme of hopping $t = 0$ (dice lattice) and $t' = 0$ (honeycomb lattice), there is a completely flat band intersecting the Dirac points at zero energy. The flat band in the limit $t' = 0$ is formed by isolated sites, thus is trivial compared to that of the dice lattice.

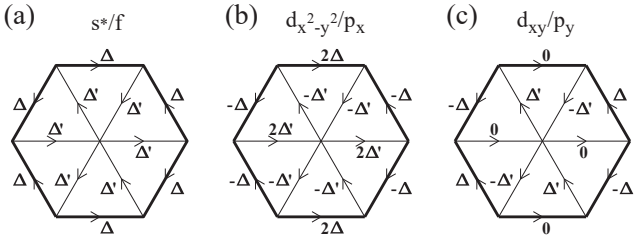

FIG. 2. The pairing symmetries considered in this paper. A partner down spin fermion is created on the six nearest-neighbor sites of the up spin fermion placed at the hexagon center. For triplet pairing, there is an additional sign when the pairing is along the opposite direction of the arrow.

Pairing symmetries and mean-field description of the superconducting state- In the presence of on-site repulsive interactions, pairing has to be nonlocal. One can consider a collection of operators Δ^α which create an up spin electron on a site, with a surrounding cloud of down spin electrons on its near-neighbors. The pairing symmetries should be in compatable with the underlying lattice. The form of the self-consistent BCS gap equation $\Delta_k = -\sum_{k'} \Gamma_{kk'} (\Delta_{k'}/2E_{k'}) \tanh(E_{k'}/2T)$ for $\Gamma_{kk'} > 0$ suggests that only solutions Δ_k which change sign (have nodes) in momentum space are allowed[33]. Although the pairing amplitudes will differ on strong and weak bonds due to the hopping modulation, the symmetry remains that of the triangle lattice, i.e. described by the crystal symmetry group D_{6h} with $k_z = 0$. The possible pairing states can be classified by the irreducible representations of D_{6h}, and include the singlet pairing symmetries: s^*-wave, $d_{x^2-y^2}$-wave, d_{xy}-wave, and triplet pairing symmetries: p_x-wave, p_y-wave, f-wave. These are schematically shown in Fig. 2. Since $d_{x^2-y^2}, d_{xy}$ (p_x, p_y) belong to the

same representation E_{2g} (E_{1u}), they are degenerate, and a linear combination of them is possible when it is energetically favored.

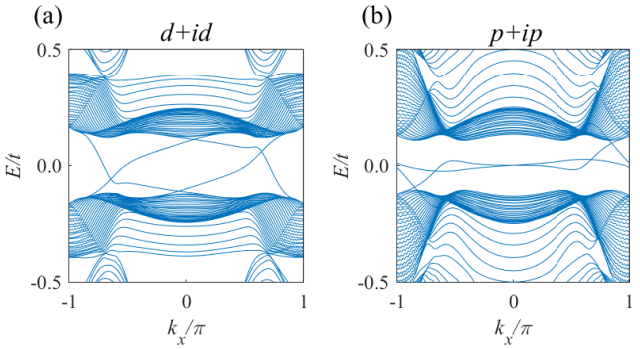

FIG. 3. The quasiparticle spectrum on zigzag edge ribbon: (a), the $d+id$ chiral superconducting state; (b), the triplet $p+ip$ state. The parameters are $t'/t = 0.3, \Delta = 0.3, \Delta' = 0.1$ and $\mu = 0.22$ (corresponding to $\rho = 0.94$).

In the Nambu representation, the superconducting Hamiltonian in mean-field theory is,

$$H_{SC} = \sum_{\mathbf{k}} \Psi^{\dagger}_{\mathbf{k}} \mathcal{H}_{\mathbf{k}} \Psi_{\mathbf{k}}, \tag{3}$$

with $\Psi_{\mathbf{k}} = (c_{A,\mathbf{k}\uparrow}, c_{B,\mathbf{k}\uparrow}, c_{C,\mathbf{k}\uparrow}, c^{\dagger}_{A,-\mathbf{k}\downarrow}, c^{\dagger}_{B,-\mathbf{k}\downarrow}, c^{\dagger}_{C,-\mathbf{k}\downarrow})^T$ and

$$\mathcal{H}_{\mathbf{k}} = \begin{pmatrix} \mathcal{H}_0(\mathbf{k}) - \mu & \Delta^{\dagger}_{\mathbf{k}} \\ \Delta_{\mathbf{k}} & -\mathcal{H}_0(\mathbf{k}) + \mu \end{pmatrix}, \tag{4}$$

$$\Delta_{\mathbf{k}} = \begin{pmatrix} 0 & \eta_{\mathbf{k}} & \zeta\eta'^{*}_{\mathbf{k}} \\ \zeta\eta^{*}_{\mathbf{k}} & 0 & \eta'_{\mathbf{k}} \\ \eta'_{\mathbf{k}} & \zeta\eta'^{*}_{\mathbf{k}} & 0 \end{pmatrix}.$$

Here μ is the chemical potential. $\eta_{\mathbf{k}} = \sum_j \Delta_j e^{i\mathbf{k}\cdot\mathbf{e}_j}$ and $\eta'_{\mathbf{k}} = \sum_j \Delta'_j e^{i\mathbf{k}\cdot\mathbf{e}_j}$, with pairing amplitudes Δ_j and Δ'_j which can be read from the real space arrangement in Fig. 2; $\zeta = -1(+1)$ for singlet (triplet) pairing. In the presence of these more complex interband pairings, the quasiparticle spectrum does not follow the standard BCS form, and it is not straightforward to identify whether there are zero-energy quasiparticles. By numerically diagonalizing the Hamiltonian Eq. (4), it is found that the s^*-wave state is fully gapped, and the triplet f-wave state has nodes.

Although the $d_{x^2-y^2}$- and d_{xy}-wave pairings are gapless, the chiral one arising from their linear combination is gapped. The chiral state is a topological superconductor characterized by an integer Chern number[34],

$$C = \sum_{n}^{occ.} \frac{1}{2\pi} \int_{BZ} dk_x dk_y F_n, \tag{5}$$

$$F_n = (\bigtriangledown \times \mathbf{A}_n)_z, \mathbf{A}_n = i\langle u_{n\mathbf{k}} | \frac{\partial}{\partial \mathbf{k}} | u_{n\mathbf{k}} \rangle.$$

Using a gauge-independent method, the Chern number can be directly calculated numerically[35]. $C = 2$ for the $d_{x^2-y^2} + id_{xy}$ state. In the presence of edges, gapless states appear which tranverse the gap (see Fig. 3). The triplet chiral $p+ip$-wave state is also topological, with $C = 1$.

With this general mean field insight in hand, we turn now to an explicit evaluation of the superconducting correlation functions in the different pairing channels.

DQMC study of the dominating pairing symmetry.- The Hubbard model Eq. (1) can be solved numerically by means of the DQMC method[26,36]. In this approach, one decouples the on-site interaction term through the introduction of an auxiliary Hubbard-Stratonovich field (HSF). The fermions are integrated out analytically, and then the integral over the HSF is performed stochastically. The only errors are those associated with the statistical sampling, the finite spatial lattice and inverse temperature discretization. All are well-controlled in the sense that they can be systematically reduced as needed, and further eliminated by appropriate extrapolations. The systems we studied have $N = 3 \times L \times L$ sites with L up to 10. The sign problem[22–24] limits accessible temperatures unless special symmetries prevent the product of determinants, which serves as the HSF probability, from becoming negative.

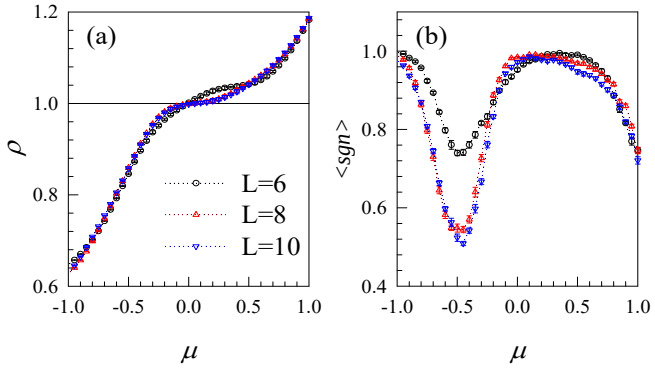

FIG. 4. The (a) density and (b) average sign as functions of μ for linear lattice sizes $L = 6, 8, 10$. Here $U = 2, T = 1/12$ and $t'/t = 0.3$. From (a) we see a clear indication of the formation of a insulating gap at half-filling. (b) indicates that accessible temperatures will be limited to $T \gtrsim t/12$ at $\mu \sim -0.5$

Figure 4 shows the density ρ and average sign $\langle sgn \rangle$ as functions of μ at $U = 2$. At $t' = 0$, the geometry consists of a honeycomb lattice and a collection of independent sites; there is no sign problem. As t' increases, the lattice is no longer bipartite and $\langle sgn \rangle < 1$. As shown in Fig. 4(b) at $T = 1/12, U = 2, t'/t = 0.3$, $\langle sgn \rangle \gtrsim 0.6$ over the full range of densities. $\rho(\mu)$ has a flat $\rho = 1$ region near $\mu = 0$ which becomes more pronounced as the lattice size increases. This implies that the system exhibits an insulating phase at half filling, with the gap size $\Delta_{\rm sp} \sim 0.5t$ set by the width of the $\rho = 1$ plateau. (This value is of the same order of magnitude as found in the Bernal case $\Delta_{\rm sp} \sim 0.3t$ at $U = 4$ and $t' = t$. See Ref.[11].) The correlated insulator behavior is consis-

tent with that recently observed in magic-angle graphene superlattices[17], indicating the model of Eq. (1) captures one of the key experimental features. A (Slater) gap appears at weak coupling also for a square lattice. Its origin there is in the AFLRO which onsets for any $U > 0$ owing to Fermi surface nesting. For generic geometries without AFLRO, a non-zero U_c, set by the bandwidth, is required to enter the Mott phase. Here the flatness of the central band induces strong correlation physics even at small values of U relative to the total bandwidth.

Short range antiferromagnetic correlations are also present, as seen in Fig. 5. Values are identical in the triangular lattice limit $t' = t$. m_t grows steadily in magnitude as t', and hence frustration, are reduced. $m_{t'}$ decreases with weakening t' [Fig. 5(a)]. Data for m_t at $\rho = 0.94$ and $\rho = 1.06$ are virtually indistinguishable. However, at $t'/t = 0.3$, $m_{t'}$ is roughly three times larger in magnitude for dopings below $\rho = 1$ than for dopings above $\rho = 1$ [Fig. 5(b)]. This suggests a similar asymmetry might occur for superconductivity which plays off magnetic fluctuations.

To determine the dominating pairing symmetry, we evaluate the uniform pairing susceptibility,

$$\chi^\alpha = \frac{1}{N}\int_0^\beta d\tau \sum_{ij} \langle \Delta_i^\alpha(\tau)\Delta_j^{\alpha\dagger}(0)\rangle\,, \qquad (6)$$

The time dependent pairing operator $\Delta_i^\alpha(\tau) = \sum_j f_{ij}^\alpha e^{\tau H} c_{i\uparrow} c_{j\downarrow} e^{-\tau H}$ with $f_{ij}^\alpha = 0, \pm 1$ or ± 2 for the bond connecting i and j, depending on the pairing symmetry α (Fig. 2). The effective susceptibility $\chi_{\rm eff}^\alpha = \chi^\alpha - \chi_0^\alpha$, subtracts the uncorrelated part χ_0^α from χ^α, thereby more directly measuring the enhancement due to U. $\chi_{\rm eff}^\alpha$ can be used to evaluate the pairing vertex[33,37].

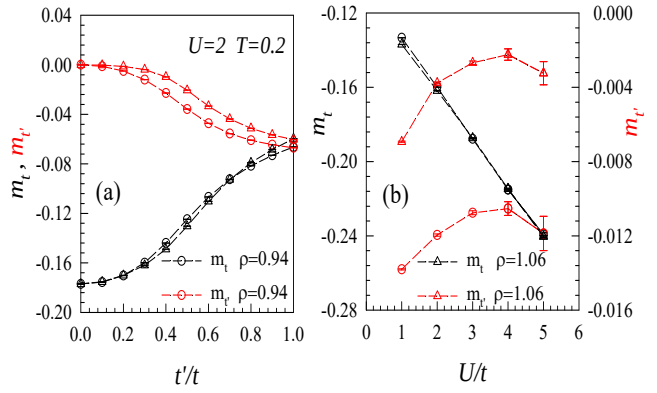

FIG. 5. The near-neighbor spin correlations $m_{t'}$ and m_t along the t' and t bonds respectively. (a) as a function of t'/t for fixed $U = 2$. (b) As a function of U for fixed $t'/t = 0.3$. The temperature $T = 0.2t$. Results for densities on either side of half-filling are shown.

Figure 6 shows $\chi_{\rm eff}^\alpha$ vs temperature for different pairing channels at $\rho = 0.94$ and $\rho = 1.06$ for $U = 2$ and $t'/t = 0.3$. The values for triplet p- and f-wave pairings are negative (repulsive); those of the corresponding singlet

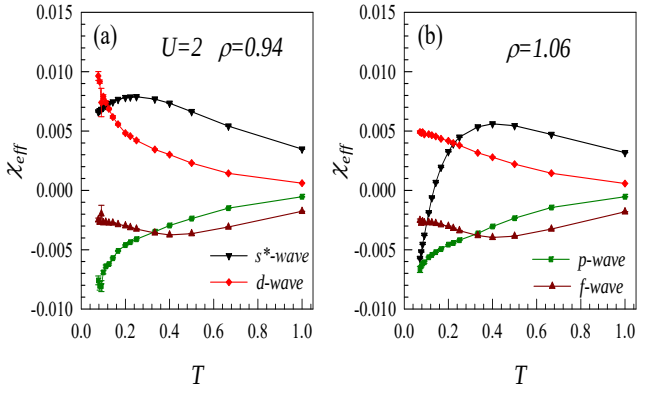

FIG. 6. The effective pairing susceptibility at $\rho = 0.94$ as a function of temperature for different pairing channels. Here $U = 2$ and the lowest temperature accessed by DQMC is $T = 1/13$. Here $\Delta'/\Delta = 0.3$ and the results are similar for other ratios.

s^*- and d- channels are positive (attractive). Moreover, $\chi_{\rm eff}^d$ increases rapidly at low temperatures (in contrast to the behaviour of $\chi_{\rm eff}^{s*}$.

$\chi_{\rm eff}$ cannot distinguish degenerate symmetries, such as $d_{x^2-y^2}, d_{xy}$ and p_x, p_y. Linear combinations will have the same $\chi_{\rm eff}$. To determine the optimal pairing symmetry, an analysis of the Ginzburg-Landau free energy such as in Ref.[19] should be performed. From our finite lattice DQMC results, where no spontaneous symmetry breaking is possible, we can infer only that a chiral $d_{x^2-y^2} + id_{xy}$ symmetry is a candidate phase. A qualitative argument in favor of the chiral phase is that it allows a non-trivial solution of the gap equation (see discussion above), while leaving the gap everywhere large. This suggests it might be energetically favored[33].

Conclusions.- The appropriate lattice geometry (band structure) and nature of interactions that need to be incorporated in a Hamiltonian describing superconductivity in twisted bilayer graphene are, of course, uncertain at this point. Suggestions include bilayer triangular and honeycomb models[21,38–40], and interactions which have SU(4) intra and inter-orbital symmetry. Studies starting from a continuum model[41] or considering other pairing mechanisms[42] have also appeared. The situation parallels that following the discovery of cuprate superconductivity, where single band (square lattice) models contended alongside three band (CuO_2) models, and both on-site U (spin fluctuation) and inter-band V (charge fluctuation) mechanisms were explored.

In this work, we have studied the pairing symmetry of a triangular lattice Hubbard Hamiltonian with modulated hoppings using the DQMC method. We first argued that the band structure of this model incorporates a nearly-flat low energy band, which underlies the physics of the graphene superlattice, and then demonstrated that insulating behavior occurs at weak interactions. Among the pairing symmetries allowed by the triangular symmetry, the dominating pairing channels are linear com-

binations of the degenerate $d_{x^2-y^2}$ and d_{xy} symmetries, including $d_{x^2-y^2}+id_{xy}$ pairing, a form which is topological and characterized by an integer topological invariant and gapless edge states.

Acknowledgments.- The authors thank W. Pickett for helpful information. H.G. acknowledges support from NSFC grant No. 11774019. X.Z. and S.F. are supported by the National Key Research and Development Program of China under Grant No. 2016YFA0300304, and NSFC under Grant Nos. 11574032 and 11734002. The work of R.T.S. is supported by DOE grant No. DE-SC0014671.

Appendix A: Evolution of the band structure

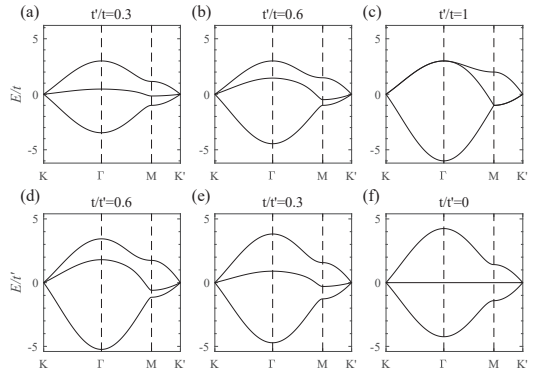

FIG. 7. The evolution of the band structure as a function of the anisotropic ratio t'/t.

The band structure evolves with the anisotropic ratio t'/t, which is shown explicitly in Fig.7. For $t' < t$ the trivial flat band disperses as t'/t increases. The $t = 0$ limit is the dice lattice and the Hamiltonian in the momentum space writes as,

$$\mathcal{H}_0^{dice}(\mathbf{k}) = \begin{pmatrix} 0 & 0 & -t'\gamma_{\mathbf{k}}^* \\ 0 & 0 & -t'\gamma_{\mathbf{k}} \\ -t'\gamma_{\mathbf{k}} & -t'\gamma_{\mathbf{k}}^* & 0 \end{pmatrix}. \qquad \text{(A1)}$$

The energy spectrum contains three branches: $E_{\mathbf{k}}^{1(2)} = \pm\sqrt{2}t'|\gamma_{\mathbf{k}}|$ and $E_{\mathbf{k}}^3 = 0$. The flat band also disperses for $t/t' \neq 0$. At $t = t'$ the band structure becomes that of the triangle lattice.

Appendix B: The superconducting order parameter

When $t = t'$, the geometry is the normal triangle lattice. The superconducting Hamiltonian in the momentum space is,

$$\mathcal{H}_{\mathbf{k}}^t = \begin{pmatrix} \mathcal{H}_0^t(\mathbf{k}) - \mu & \Delta_{\mathbf{k}}^{t\dagger} \\ \Delta_{\mathbf{k}}^t & -\mathcal{H}_0^t(\mathbf{k}) + \mu \end{pmatrix}, \qquad \text{(B1)}$$

Here the noninteracting Hamiltonian is $\mathcal{H}_0^t(\mathbf{k}) = -t(\gamma_{\mathbf{k}} + \gamma_{\mathbf{k}}^*)$. The superconducting order parameter is $\Delta_{\mathbf{k}}^t = \sum_{j=1}^3 \Delta_j(e^{i\mathbf{k}\cdot\mathbf{e}_j} + \zeta e^{-i\mathbf{k}\cdot\mathbf{e}_j})$ with pairing amplitudes Δ_j which can be read from the real space arrangement in Fig. 2; $\zeta = 1(-1)$ for singlet (triplet) pairing. Figure 8 shows the momentum dependence of $\Delta_{\mathbf{k}}^t$, which is consistent with the symmetries of the corresponding pairing channels.

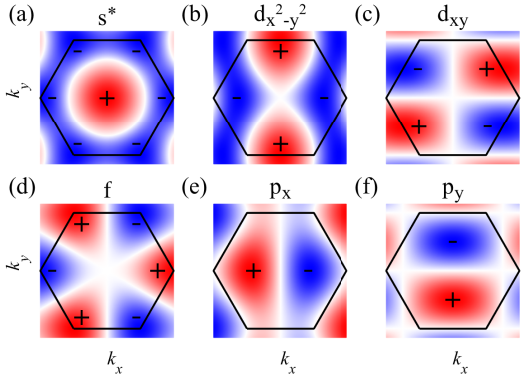

FIG. 8. The momentum dependence of $\Delta_{\mathbf{k}}^t$ for s^*, $d_{x^2-y^2}$, d_{xy}, f, p_x, p_y pairing channels.

For the case $t' \neq t$, it is expected that the pairing amplitude Δ' on bonds with t' should be different from that on bonds with the hopping amplitude t. However the ratio Δ'/Δ can not be determined by our method. We calculate the effective susceptibility for different values of Δ'/Δ and find that the d-wave phase is always dominate(see Fig.9).

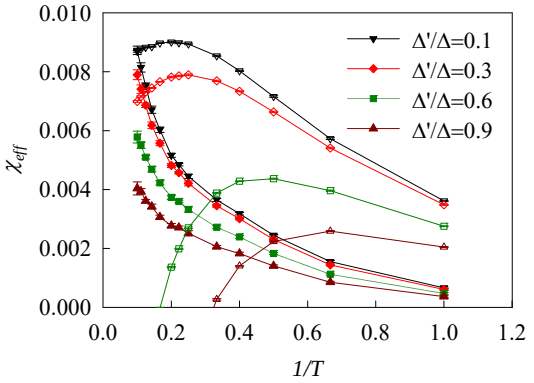

FIG. 9. The effective susceptibility at different Δ'/Δ for s^*-, d-wave pairing channels. The filled (open) symbols represent d-(s^*-)wave pairing phases. The f- and p-wave phases have smaller χ_{eff}, and are not shown here. The filling is $\rho = 0.94$.

[1] R. Bistritzer and A. H. MacDonald, Phys. Rev. B **81**, 245412 (2010).
[2] G. Trambly de Laissardière, D. Mayou, and L. Magaud, Phys. Rev. B **86**, 125413 (2012).
[3] G. Trambly de Laissardire, D. Mayou, and L. Magaud, Nano Letters **10**, 804 (2010), pMID: 20121163, https://doi.org/10.1021/nl902948m.
[4] K. V. Emtsev, F. Speck, T. Seyller, L. Ley, and J. D. Riley, Phys. Rev. B **77**, 155303 (2008).
[5] M. Sprinkle, D. Siegel, Y. Hu, J. Hicks, A. Tejeda, A. Taleb-Ibrahimi, P. Le Fèvre, F. Bertran, S. Vizzini, H. Enriquez, S. Chiang, P. Soukiassian, C. Berger, W. A. de Heer, A. Lanzara, and E. H. Conrad, Phys. Rev. Lett. **103**, 226803 (2009).
[6] J. Hicks, M. Sprinkle, K. Shepperd, F. Wang, A. Tejeda, A. Taleb-Ibrahimi, F. Bertran, P. Le Fèvre, W. A. de Heer, C. Berger, and E. H. Conrad, Phys. Rev. B **83**, 205403 (2011).
[7] D. Miller, K. Kubista, G. Rutter, M. Ruan, W. de Heer, P. First, and J. Stroscio, Science **324**, 924 (2009).
[8] C. Berger, Z. Song, X. Li, X. Wu, N. Brown, C. Naud, D. Mayou, T. Li, J. Hass, A. N. Marchenkov, E. H. Conrad, P. N. First, and W. A. de Heer, Science **312**, 1191 (2006).
[9] M. L. Sadowski, G. Martinez, M. Potemski, C. Berger, and W. A. de Heer, Phys. Rev. Lett. **97**, 266405 (2006).
[10] M. J. Gilbert and J. Shumway, Journal of Computational Electronics **8**, 51 (2009).
[11] T. C. Lang, Z. Y. Meng, M. M. Scherer, S. Uebelacker, F. F. Assaad, A. Muramatsu, C. Honerkamp, and S. Wessel, Phys. Rev. Lett. **109**, 126402 (2012).
[12] S. Pujari, T. C. Lang, G. Murthy, and R. K. Kaul, Phys. Rev. Lett. **117**, 086404 (2016).
[13] H.-S. Tao, Y.-H. Chen, H.-F. Lin, H.-D. Liu, and W.-M. Liu, Nature Scientific Reports **4**, 5367 (2014).
[14] H. Tang, Ph.D. thesis (2017).
[15] T. Paiva, R. T. Scalettar, W. Zheng, R. R. P. Singh, and J. Oitmaa, Phys. Rev. B **72**, 085123 (2005).
[16] Y. Otsuka, S. Yunoki, and S. Sorella, Phys. Rev. X **6**, 011029 (2016).
[17] Y. Cao, V. Fatemi, A. Demir, S. Fang, S. L. Tomarken, J. Y. Luo, J. D. Sanchez-Yamagishi, K. Watanabe, T. Taniguchi, E. Kaxiras, R. C. Ashoori, and P. Jarillo-Herrero, Nature (2018), doi:10.1038/nature26154.
[18] Y. Cao, V. Fatemi, S. Fang, K. Watanabe, T. Taniguchi, E. Kaxiras, and P. Jarillo-Herrero, Nature (2018), doi:10.1038/nature26160.
[19] R. Nandkishore, L. Levitov, and A. Chubukov, Nature Physics **8**, 158 (2012).
[20] S. Pathak, V. B. Shenoy, and G. Baskaran, Phys. Rev. B **81**, 085431 (2010).
[21] C. Xu and L. Balents, arXiv:1803.08057.
[22] E. Y. Loh, J. E. Gubernatis, R. T. Scalettar, S. R. White, D. J. Scalapino, and R. L. Sugar, Phys. Rev. B **41**, 9301 (1990).
[23] M. Troyer and U.-J. Wiese, Phys. Rev. Lett. **94**, 170201 (2005).
[24] V. I. Iglovikov, E. Khatami, and R. T. Scalettar, Phys. Rev. B **92**, 045110 (2015).
[25] D. J. Scalapino, E. Loh, and J. E. Hirsch, Phys. Rev. B **34**, 8190 (1986).
[26] S. R. White, D. J. Scalapino, R. L. Sugar, N. E. Bickers, and R. T. Scalettar, Phys. Rev. B **39**, 839 (1989).
[27] S. R. White, D. J. Scalapino, R. L. Sugar, E. Y. Loh, J. E. Gubernatis, and R. T. Scalettar, Phys. Rev. B **40**, 506 (1989).
[28] R. Bistritzer and A. H. MacDonald, PNAS **108**, 12233 (2011).
[29] G. Trambly de Laissardière, D. Mayou, and L. Magaud, Phys. Rev. B **86**, 125413 (2012).
[30] G. Baskaran, arXiv:1804.00627.
[31] A. Ramires and J. L. Lado, arXiv:1803.04400.
[32] S.-Y. Li, K.-Q. Liu, L.-J. Yin, W.-X. Wang, W. Yan, X.-Q. Yang, J.-K. Yang, H. Liu, H. Jiang, and L. He, Phys. Rev. B **96**, 155416 (2017).
[33] D. J. Scalapino, Phys. Rep. **250**, 329 (1995).
[34] A. P. Schnyder, S. Ryu, A. Furusaki, and A. W. W. Ludwig, Phys. Rev. B **78**, 195125 (2008).
[35] T. Fukui, Y. Hatsugai, and H. Suzuki, J. Phys. Soc. Jpn. **74**, 1674 (2005).
[36] R. Blankenbecler, D. J. Scalapino, and R. L. Sugar, Phys. Rev. D **24**, 2278 (1981).
[37] E. Khatami, R. T. Scalettar, and R. R. P. Singh, Phys. Rev. B **91**, 241107 (2015).
[38] H. Po, L. Zou, A. Vishwanath, and T. Senthil, arXiv:1803.09742.
[39] N. F. Q. Yuan and L. Fu, arXiv:1804.09699.
[40] X.-Y. Xu, K. T. Law, and P. A. Lee, arXiv:1805.00478.
[41] B. Roy and V. Juricic, arXiv:1803.11190.
[42] B. Padhi, C. Setty, and P. W. Phillips, arXiv:1804.01101.